Letter

Measurement of the Born cross section for $e^+e^- \to \eta h_c$ at center-of-mass energies between 4.1 and 4.6 GeV

M. Ablikim *et al.*[*]
(BESIII Collaboration)

(Received 10 April 2024; revised 30 August 2024; accepted 13 December 2024; published 8 January 2025)

We measure the Born cross section for the reaction $e^+e^- \to \eta h_c$ from $\sqrt{s} = 4.129$ to 4.600 GeV using datasets collected by the BESIII detector running at the BEPCII collider. A resonant structure in the cross-section line shape near 4.200 GeV is observed with a statistical significance of 7σ. The parameters of this resonance are measured to be $M = 4188.8 \pm 4.7 \pm 8.0\ \mathrm{MeV}/c^2$ and $\Gamma = 49 \pm 16 \pm 19$ MeV, where the first uncertainties are statistical and the second systematic.

DOI: 10.1103/PhysRevD.111.L011101

In recent years, several new vector resonances, including the $\psi(4230)$, $\psi(4360)$, and $\psi(4660)$, have been observed in the charmonium region at B-factories and τ-charm factories [1–3]. While the potential models [4] can accommodate the $\psi(4040)$, $\psi(4160)$, and $\psi(4415)$, the new states appear to be supernumerary. These vector states, also known as $Y(m)$, will be referred to as $\psi(m)$ throughout this paper. Several models have been proposed to explain them as exotic non-$c\bar{c}$ mesons [5–9]. The nature of the first observed vector charmoniumlike state, the $\psi(4230)$ is still mysterious. It is regarded as a good candidate for a hybrid state because its mass is close to the vector hybrid state predicted by lattice QCD [10] and also because of its small electronic width [11,12] and decay pattern [13]. But it is also interpreted as a conventional charmonium [14–16], hadronic molecule [17,18], nonresonant enhancement [19]. More experimental measurements are valuable to elucidate the nature of the $\psi(4230)$.

Recently, BESIII precisely measured the cross sections for $e^+e^- \to \pi^+\pi^- J/\psi$ [20] and $e^+e^- \to \pi^+\pi^- h_c$ [21], observing a double-resonance structure in both processes. Following these studies, BESIII explored various other processes, including $e^+e^- \to K\bar{K}J/\psi$ [22,23], $\pi^+\pi^-\psi(3686)$ [24], $\eta J/\psi$ [25], $\omega\chi_{c0}$ [26], $\pi^+D^0D^{*-}$ [27], and $D_s^{*+}D_s^{*-}$ [28], to search for vector charmonium(like) states through their production cross sections. Although similar resonant structures around 4.2 GeV were observed across these processes, the measured resonant parameters varied depending on the process. This discrepancy could be attributed to coupled-channel effects, interferences between different resonances, and parametrizations of cross-section line shapes. Therefore, a more integrated approach, such as a coupled-channel analysis, is necessary to achieve a consistent description of these states. Measuring more decay modes of $\psi(4230)$ is crucial for such a study, as including a wide range of channels can enhance the predictive power of coupled-channel models.

Studying transitions from vector states to the h_c meson is intriguing because a strong coupling to h_c suggests a hybrid state with a $c\bar{c}$ pair in a spin-singlet configuration [29]. The process $e^+e^- \to \eta h_c$ was first observed at $\sqrt{s} = 4.226$ GeV by BESIII using 2012–2014 data [30], hinting at a structure around 4.200 GeV. Recently, BESIII collected more data at c.m. energies from 4.129 to 4.600 GeV. In this paper, we use these new datasets to update the study of $e^+e^- \to \eta h_c$ with $h_c \to \gamma\eta_c$ and $\eta \to \gamma\gamma$, significantly improving our cross-section measurement. The total integrated luminosity is measured to be $\sim 15\ \mathrm{fb}^{-1}$ using large-angle Bhabha scattering events with an uncertainty of 1.0% [31], and the c.m. energies are measured using the dimuon process [32].

The BESIII detector is described in detail elsewhere [33]. The determination of the detection efficiency and estimation of physics backgrounds are carried out with Monte Carlo (MC) samples. Geant4-based [34,35] detector simulation software is used to model the detector response. The signal MC events are simulated for each decay mode of the η_c meson with KKMC [36] and BesEvtGen [37], in which the line shape of the η_c is modeled according to a Breit-Wigner (BW) function. The $e^+e^- \to \eta h_c$ process is assumed to be dominated by the S wave, and the E1 transition $h_c \to \gamma\eta_c$ is simulated using a dedicated helicity formalism [38]. In order to study potential backgrounds, inclusive MC samples are simulated at each c.m. energy with KKMC.

In this measurement, we reconstruct all the particles in the final state, including the bachelor η in $e^+e^- \to \eta h_c$, the photon in the E1 transition $h_c \to \gamma\eta_c$, and η_c, which is

[*]Full author list given at the end of the Letter.

reconstructed with sixteen hadronic final states with a total branching fraction of about 40%: $p\bar{p}$, $2(\pi^+\pi^-)$, $2(K^+K^-)$, $K^+K^-\pi^+\pi^-$, $p\bar{p}\pi^+\pi^-$, $3(\pi^+\pi^-)$, $K^+K^-2(\pi^+\pi^-)$, $K^+K^-\pi^0$, $p\bar{p}\pi^0$, $K^0_S K^\pm\pi^\mp$, $K^0_S K^\pm\pi^\mp\pi^\pm\pi^\mp$, $\pi^+\pi^-\eta$, $K^+K^-\eta$, $2(\pi^+\pi^-)\eta$, $\pi^+\pi^-\pi^0\pi^0$, and $2(\pi^+\pi^-)\pi^0\pi^0$. The η/π^0 candidates are reconstructed using two photons and the K^0_S candidates are reconstructed via the $\pi^+\pi^-$ decay channel. For the selected candidates, we apply a fit to the distribution of the η recoil mass to obtain the ηh_c signal yield.

The selection criteria for charged tracks and photon candidates as well as the π^0, η and K^0_S reconstruction are described in Ref. [30]. After that, a four-constraint (4C) kinematic fit is performed for each event imposing overall energy-momentum conservation, and the χ^2_{4C} is required to be below a certain threshold to suppress background events. The best candidates of π^0, η and K^0_S as well as the particle identification (PID) assignments of charged tracks in an event are determined by minimizing $\chi^2 \equiv \chi^2_{4C} + \chi^2_{1C} + \chi^2_{\rm PID} + \chi^2_{\rm vertex}$, where χ^2_{1C} is the overall χ^2 of the 1C fit for all π^0 and η candidates, $\chi^2_{\rm PID}$ is the sum over all charged tracks of the χ^2 of the PID hypotheses, and $\chi^2_{\rm vertex}$ is the χ^2 of the K^0_S secondary-vertex fit. If there is no π^0 (K^0_S) in an event, the corresponding χ^2_{1C} ($\chi^2_{\rm vertex}$) is set to zero. If multiple η candidates are found with recoil masses within the h_c preselection signal region of $[3.40, 3.65]$ GeV/c^2, the candidate with a mass closest to the known η_c mass is selected as the daughter particle of η_c.

The requirements on χ^2_{4C} and the mass windows for the η and η_c selections are determined by maximizing a figure of merit, which is defined as $S/\sqrt{S+B}$. Here, S and B are the signal and background yields, respectively. The optimization was performed using the combined size of four samples with high integrated luminosity taken at $\sqrt{s} = 4.179$, 4.189, 4.199, and 4.209 GeV.

After applying all the above criteria and using a h_c mass window of $[3.510, 3.540]$ GeV/c^2, a clear η_c signal is observed in the invariant mass spectrum of hadrons in the data sample taken at $\sqrt{s} = 4.179$ GeV, which is shown in the left panel of Fig. 1. A clear h_c signal is also seen in the η recoil mass distribution when applying a mass window of $[2.944, 3.024]$ GeV/c^2 to the invariant mass distribution of hadrons from η_c decay, as shown in the right panel of Fig. 1. The two-dimensional distributions of η recoil mass versus the invariant mass spectrum of hadrons are shown in the Supplemental Material [39].

In the η recoil mass spectra, as depicted in Fig. 1 (right), no peaking structures are observed within the η_c sidebands, which are delineated as $[2.870, 2.910]$ GeV/c^2 and $[3.050, 3.090]$ GeV/c^2, as demonstrated in Fig. 1 (left). Likewise, the hadronic invariant mass spectrum resulting from η_c decay within the h_c sidebands, specified as $[3.490, 3.505]$ GeV/c^2 and $[3.545, 3.560]$ GeV/c^2, exhibits no peak formations, as illustrated in Fig. 1 (left). In addition, inclusive MC samples simulated at $\sqrt{s} = 4.179$ GeV

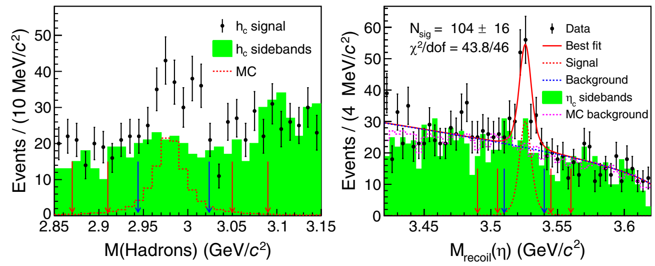

FIG. 1. Left: combined invariant mass distribution of the sixteen hadronic final states forming the η_c meson in the h_c signal (dots with error bars) and sideband ranges (green shaded histogram) at $\sqrt{s} = 4.179$ GeV. The dashed red histogram represents simulation results. Blue arrows indicate the η_c signal region; red arrows indicate sidebands. Right: sum of simultaneous fits to the η recoil mass spectra for all sixteen η_c decay modes at $\sqrt{s} = 4.179$ GeV. Dots with error bars represent data. The solid red line shows the total fit; dashed red and blue lines show signal and background components. Green-shaded histogram shows η_c sidebands. Dashed pink line is the background from inclusive MC sample. Blue arrows define the h_c signal region; red arrows indicate sidebands.

are analyzed with the same event selection as applied to data and the dominant background is found to be the continuum processes. The contribution of other sources is negligible. The comparison between data and the inclusive MC sample is shown in Fig. 1 (right).

To obtain the h_c yield, the sixteen η recoil mass distributions are fitted simultaneously with an unbinned maximum extended-likelihood method. In the fit, the signal shape is determined by MC simulation, and the background is described by an ARGUS function [40]. The kinematic limit of the invariant mass distribution is set to be the same for all channels and fixed according to simulation at each c.m. energy. The total signal yield, $N_{\rm sig}$, is the sum of the yields from all the sixteen η_c decay channels. The signal yield of the ith channel is set to be $N_{\rm sig} \cdot f_i$, where f_i is the weight factor $f_i = \epsilon_i \mathcal{B}_i / \sum \epsilon_i \mathcal{B}_i$, $\mathcal{B}_i$ denotes the branching fraction of η_c decays to the ith final state and ϵ_i is the corresponding efficiency. The fraction of the background in each mode is allowed to vary freely. The sum of the fit results at $\sqrt{s} = 4.179$ GeV is shown in Fig. 1 (right). We bin the $\mathrm{M}_{\rm recoil}(\eta)$ distribution and define a χ^2-like quantity based on the (unbinned) fit results to obtain an approximate assessment of the goodness of fit, $\chi^2/\mathrm{dof} = 43.8/46$, where dof are the degrees of freedom. The total signal yield is 104 ± 16 with a statistical significance of 8.8σ, which is obtained by comparing the change of the log-likelihood value $\Delta(-\ln L) = 39$ and degrees of freedom $\Delta\mathrm{dof} = 1$ with and without h_c signal in the fit. Using the same method, we also study the data samples taken at other c.m. energies. Significant signals ($\sim 5\sigma$ or above) are observed at $\sqrt{s} = 4.179$, 4.189, and 4.226 GeV, and evidence (between 3σ and 5σ) is found at $\sqrt{s} = 4.209$, 4.358 and 4.436 GeV.

The Born and "dressed" cross sections are calculated by the following formula:

$$\sigma^{\mathrm{Born}} = \frac{\sigma^{\mathrm{dressed}}}{\frac{1}{|1-\Pi|^2}} = \frac{N_{\mathrm{sig}}}{\mathcal{L}(1+\delta)\frac{1}{|1-\Pi|^2}\mathcal{B}_\eta \mathcal{B}_{h_c}\Sigma_i \epsilon_i \mathcal{B}_i}, \quad (1)$$

where $\mathcal{L}$ is the integrated luminosity of the data sample taken at each c.m. energy. The radiative correction factor $(1+\delta)$ at each c.m. energy is calculated iteratively [30]. The term $\frac{1}{|1-\Pi|^2}$ is the vacuum-polarization (VP) correction factor and is calculated according to Ref. [41]. In addition, $\mathcal{B}_\eta$ and $\mathcal{B}_{h_c}$ are the branching fractions of the $\eta \to \gamma\gamma$ and $h_c \to \gamma\eta_c$ decays, respectively, and ϵ_i is the efficiency determined with MC simulation. The measured Born cross sections and the quantities relevant to the calculation at all c.m. energies are listed in the Supplemental Material [39].

The cross section of $e^+e^- \to \eta h_c$ from $\sqrt{s} = 4.129$ to 4.600 GeV is parametrized as $\sigma^{\mathrm{dressed}}(s) = |\mathrm{BW}_1(s) + \mathrm{BW}_2(s)e^{i\phi}|^2 + |\mathrm{BW}_3(s)|^2$. The relativistic BW amplitude for a resonance $Y \to \eta h_c$ in the fit is written as

$$\mathrm{BW}(s) = \frac{\sqrt{12\pi\Gamma_{ee}\Gamma_{\mathrm{tot}}\mathcal{B}(Y\to\eta h_c)}}{s - M^2 + iM\Gamma_{\mathrm{tot}}}\sqrt{\frac{\mathrm{PS}(\sqrt{s})}{\mathrm{PS}(M)}}, \quad (2)$$

where $M, \Gamma_{\mathrm{tot}}, \Gamma_{ee}$, and $\mathcal{B}(Y\to\eta h_c)$ are the mass, full width, electronic partial width, and branching fraction of the corresponding resonance, respectively, and $\sqrt{\mathrm{PS}(\sqrt{s})/\mathrm{PS}(M)}$ is the two-body phase space factor [42]. It is important to note that the definition of Γ_{ee} includes vacuum polarization effects. Consequently, the dressed cross sections are fitted rather than the Born cross sections. A maximum likelihood fit is used to obtain the parameters of these three resonances. In the fit, the parameters of the second BW function are fixed to those of the $\psi(4360)$ due to the large uncertainty of the cross section in this region, while the other two BW functions are free. Our analysis is primarily concerned with the measurement of BW_1. Consequently, the interference effects between BW_1 and BW_3, as well as between BW_2 and BW_3, have been neglected in the nominal fit because of limited sample size in the regions of the BW_2 and BW_3 resonances. There could be multiple solutions in the fit due to interference between BW_1 and BW_2, but we vary the initial values of ϕ and only find one solution.

The fit results are shown in Fig. 2 and the fitted parameters of the BW functions are listed in Table I. The statistical significance of the first resonance is calculated to be 8σ, which is obtained by comparing the change of the log-likelihood value $\Delta(-\ln L) = 41$ and degrees of freedom $\Delta\mathrm{dof} = 4$ with and without this resonance in the fit.

To check the fit stability of the first resonance, we also use many different parametrizations, including changing the second resonant parameters to different hypotheses: $\psi(4320)$ [20], $\psi(4380)$ [24], $\psi(4390)$ [21] and removing the second resonance in the model. In addition, we also use

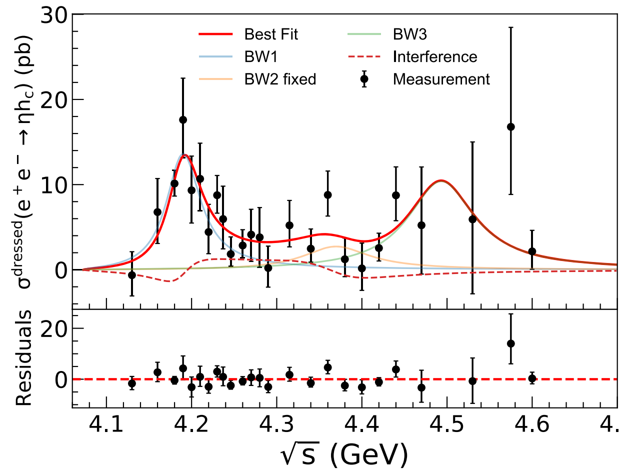

FIG. 2. Result of the nominal fit to the $\sqrt{s}$-dependent cross section $\sigma^{\mathrm{dressed}}(e^+e^- \to \eta h_c)$ with two coherent BW functions and one independent BW function. Dots with error bars are data, and the red solid curve shows the fit with three resonances. The dashed curves show the interference between BW_1 and BW_2.

the sum of a BW function and phase space shape to fit the cross section line shape and use a model that takes the interference between all three resonances into account. The comparison of the fitted line shapes of c.m. energy-dependent cross sections are shown in Supplemental Material [39]. The choice of the fit model leads to the dominant systematic uncertainties on the mass and width parameters. The significance of the first resonance remains above 7σ in all of the alternative fits.

The systematic uncertainties for the measured Born cross sections are determined as follows. The integrated luminosity is measured using Bhabha events, with an uncertainty of 1.0% [31]. To estimate the uncertainty due to the data/MC mass resolution difference in the fit to the recoil mass of η, the simulated signal shape is shifted and convolved with a Gaussian function to match the shape in the data. The parameters of the Gaussian function are obtained by a control sample of $e^+e^- \to \eta J/\psi$. The average change of the cross section with and without this correction among all the datasets is taken as the common systematic uncertainty. To estimate the uncertainty due to the background shape, a second-order Chebyshev function instead of the ARGUS function is used as an alternative

TABLE I. Results of the fit to the distribution of $\sigma^{\mathrm{dressed}}(e^+e^- \to \eta h_c)$ for the first resonance. Here, M and Γ_{tot} are the mass and the total width of the resonance. $\Gamma_{ee}\mathcal{B}$ is the product of the e^+e^- partial width and branching fraction of $Y \to \eta h_c$. The first uncertainties are statistical and the second systematic.

$\Gamma_{ee}\mathcal{B}$ (eV)	M (MeV/c^2)	Γ_{tot} (MeV)
$0.80 \pm 0.19 \pm 0.45$	$4188.8 \pm 4.7 \pm 8.0$	$49 \pm 16 \pm 19$

model. The average fit result difference between these two background shapes in all datsets is adopted as the systematic uncertainty. The systematic uncertainty from the fit range is determined by varying the fit range within 20 MeV of the nominal range and reperforming the fit, and the average difference from the nominal result among all datasets is taken as the systematic uncertainty. The branching fraction of $h_c \to \gamma\eta_c$ is taken from Ref. [43], and its uncertainty, which is 15.7%, will propagate to the cross-section measurement. The ISR correction factor at a given c.m. energy is determined using the cross-section line shape from the threshold to the c.m. energy of interest. The nominal energy-dependent cross section is parametrized with the sum of three BW functions as shown in Fig. 2. The uncertainty of the line shape is estimated by using different models as discussed in the fit to the c.m. energy-dependent cross section. The line shape of the cross section also affects the efficiency. To consider this effect, we use the method introduced in Ref. [30]. To investigate the uncertainty due to the vacuum polarization factor, we use two available VP parametrizations [41,44]. The difference between them is 0.3% and is taken as the systematic uncertainty. In the simultaneous fit to the η recoil mass distributions, $\epsilon_i\mathcal{B}_i$ is used to constrain the weights between different η_c decay modes, so the uncertainty from $\epsilon_i\mathcal{B}_i$ will affect the signal yield. To consider this issue, we use the refitting method introduced in Ref. [30] to estimate the uncertainty due to $\epsilon_i\mathcal{B}_i$. The systematic uncertainties related to efficiency including charged track, photon, K_S^0, π^0 and η reconstruction, PID, kinematic fit, η_c tag and cross feed are estimated with the same method as described in Ref. [30]. The angular momentum between the η and h_c mesons is investigated with data. However, due to the limited sample size, the data are compatible with both an S- and a D-wave assumptions. The uncertainty is estimated by comparing the efficiencies from the pure S-wave MC and a mixture of S- and D-wave MC. The uncertainties related to efficiency at $\sqrt{s} = 4.179$ GeV are given in the Supplemental Material [39].

The systematic uncertainties from different sources are listed in Table II. All sources are treated as uncorrelated, so the total systematic uncertainty is obtained by summing them in quadrature. For the datasets without significant ηh_c signals, an upper limit on the cross section at the 90% confidence level is obtained using a Bayesian method, assuming a uniform prior density. The systematic uncertainties are taken into account by convolving the probability density function of the measured cross section with a Gaussian function [45].

The systematic uncertainties for the fit parameters to the cross section line shape are described as follows. To estimate the uncertainty arising from the fit model, we use all the variations described in the fit to the c.m. energy-dependent cross section. The largest deviation is taken as the systematic uncertainty. The c.m. energies of all datasets

TABLE II. Relative systematic uncertainties on $\sigma^{\rm Born}(e^+e^- \to \eta h_c)$ (in %) at $\sqrt{s} = 4.179$ GeV.

Source	Uncertainty of $\sigma^{\rm Born}$
Luminosity	1.0
Signal shape	1.4
Background shape	7.0
Fitting range	3.6
$\mathcal{B}(h_c \to \gamma\eta_c)\mathcal{B}(\eta \to \gamma\gamma)$	15.7
ISR correction	1.9
VP correction	0.3
$\Sigma_i\epsilon_i\mathcal{B}_i$	10.4
Total	20.6

are measured using dimuon events with an uncertainty of ±1 MeV. The uncertainty of the c.m. energy measurement will propagate to the mass of the resonances directly. The uncertainty due to the beam energy spread is found to be negligible. The systematic uncertainty for the cross-section measurements can be classified into two categories: the uncertainties due to the fit, which are dataset independent and the remaining uncertainties, which are treated as correlated among all datasets. The dataset-independent uncertainties are studied by changing the configuration in the fit to the η recoil mass. We vary the signal shape, background shape and fit range for each dataset as discussed before and then redo the fit to these alternatively measured cross sections, and the largest deviations of the fitted parameters of $\mathrm{BW}_1(s)$ are taken as the systematic uncertainties. The correlated set of uncertainties would not affect the mass and width of each resonance but will propagate to the product $\Gamma_{ee}^{Y}\mathcal{B}$ by the same amount. The average of the correlated systematic uncertainty for $\Gamma_{ee}^{Y}\mathcal{B}$ is 19%. Table III summarizes the uncertainties of parameters for the resonance around $\sqrt{s} = 4.200$ GeV from the c.m. energy-dependent cross sections.

In summary, the $e^+e^- \to \eta h_c$ process is studied with the data samples taken at c.m. energies from 4.129 to 4.600 GeV. The corresponding Born cross sections or upper limits of Born cross sections at each c.m. energy are obtained. In the cross-section lineshape, a resonant structure near 4.200 GeV is observed with a statistical

TABLE III. Systematic uncertainties due to the fit of the cross-section line shape. $\sqrt{s}$ refers to c.m. energy, $\sigma_{\rm Beam}$ stands for beam energy spread, $\sigma_{\rm ind}^{\rm dressed}$ and $\sigma_{\rm cor}^{\rm dressed}$ represent the dataset independent and correlated uncertainties in the cross-section measurements.

	$\sqrt{s}$	$\sigma_{\rm Beam}$	Model	$\sigma_{\rm ind}^{\rm dressed}$	$\sigma_{\rm cor}^{\rm dressed}$	Sum
M_1 (MeV/c^2)	1.0	0.0	7.6	2.2	⋯	8.0
$\Gamma_{\rm tot}^{Y_1}$ (MeV)	⋯	0.1	17.3	8.2	⋯	19.2
$\Gamma_{ee}^{Y_1}\mathcal{B}$ (eV)	⋯	0.0	0.4	0.1	0.2	0.5

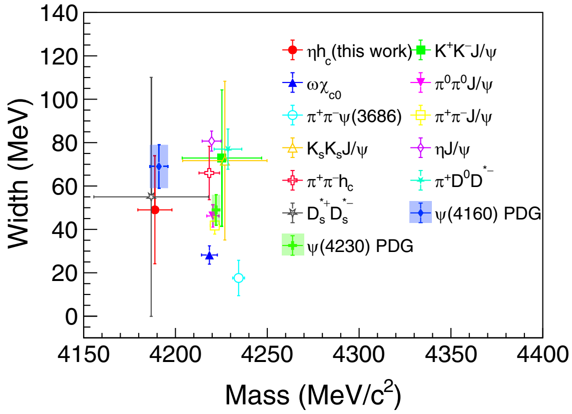

FIG. 3. Comparison of the mass and width obtained in this study with those of the $\psi(4230)$ from previous BESIII measurements [20–28], and the world average values of $\psi(4160)$ and $\psi(4230)$ as reported by the PDG [46].

significance of 7σ. The parameters of this resonance are measured to be $M = 4188.8 \pm 4.7 \pm 8.0\ \mathrm{MeV}/c^2$ and $\Gamma = 49 \pm 16 \pm 19$ MeV. Here, the first uncertainties are statistical, and the second systematic.

We compare the results from this study with those of the $\psi(4230)$ from previous BESIII measurements [20–28], and the world average values of the $\psi(4160)$ and $\psi(4230)$ [46] as shown in Fig. 3. Our results are consistent with both the parameters of $\psi(4160)$ and those of the state measured in the $e^+e^- \to D_s^{*+}D_s^{*-}$ process [28]. The mass measured in this study is lower than that of $\psi(4230)$ reported in other BESIII measurements [20–27], but the results are still consistent within three standard deviations. The 1^{--} hybrid charmonium state predicted by the BOEFT model [47] has a mass of 4.15 ± 0.15 GeV, which is consistent with our measurement. In addition, there is possible indication for two resonant structures around $\sqrt{s} = 4.3$ and 4.5 GeV. To distinguish these resonance(s) in different processes, we need not only more data but also more advanced technologies, such as coupled-channel K-matrix analysis, which is currently an ongoing effort at BESIII.

The BESIII Collaboration thanks the staff of BEPCII and the IHEP computing center for their strong support. This work is supported in part by National Key R&D Program of China under Contracts No. 2023YFA1606704, No. 2020YFA0406300, No. 2020YFA0406400; National Natural Science Foundation of China (NSFC) under Contracts No. 11635010, No. 11735014, No. 11835012, No. 11935015, No. 11935016, No. 11935018, No. 11961141012, No. 12025502, No. 12035009, No. 12035013, No. 12061131003, No. 12192260, No. 12192261, No. 12192262, No. 12192263, No. 12192264, No. 12192265, No. 12221005, No. 12225509, No. 12235017; the Chinese Academy of Sciences (CAS) Large-Scale Scientific Facility Program; the CAS Center for Excellence in Particle Physics (CCEPP); Joint Large-Scale Scientific Facility Funds of the NSFC and CAS under Contract No. U1832207; CAS Key Research Program of Frontier Sciences under Contracts No. QYZDJ-SSW-SLH003, No. QYZDJ-SSW-SLH040; 100 Talents Program of CAS; The Institute of Nuclear and Particle Physics (INPAC) and Shanghai Key Laboratory for Particle Physics and Cosmology; European Union's Horizon 2020 research and innovation programme under Marie Sklodowska-Curie grant agreement under Contract No. 894790; German Research Foundation DFG under Contracts No. 455635585, Collaborative Research Center CRC 1044, FOR5327, GRK 2149; Istituto Nazionale di Fisica Nucleare, Italy; Ministry of Development of Turkey under Contract No. DPT2006K-120470; National Research Foundation of Korea under Contract No. NRF-2022R1A2C1092335; National Science and Technology fund of Mongolia; National Science Research and Innovation Fund (NSRF) via the Program Management Unit for Human Resources & Institutional Development, Research and Innovation of Thailand under Contract No. B16F640076; Polish National Science Centre under Contract No. 2019/35/O/ST2/02907; The Swedish Research Council; U.S. Department of Energy under Contract No. DE-FG02-05ER41374.

[1] B. Aubert *et al.* (*BABAR* Collaboration), Phys. Rev. Lett. **95**, 142001 (2005).
[2] B. Aubert *et al.* (*BABAR* Collaboration), Phys. Rev. Lett. **98**, 212001 (2007).
[3] X. L. Wang *et al.* (Belle Collaboration), Phys. Rev. Lett. **99**, 142002 (2007).
[4] T. Barnes, S. Godfrey, and E. S. Swanson, Phys. Rev. D **72**, 054026 (2005).
[5] F. E. Close and P. R. Page, Phys. Lett. B **628**, 215 (2005).
[6] D. Ebert, R. N. Faustov, and V. O. Galkin, Phys. Lett. B **634**, 214 (2006).
[7] X. Liu, X.-Q. Zeng, and X.-Q. Li, Phys. Rev. D **72**, 054023 (2005).
[8] H. X. Chen, L. Maiani, A. D. Polosa, and V. Riquer, Eur. Phys. J. C **75**, 550 (2015).
[9] D. V. Bugg, J. Phys. G **35**, 075005 (2008).
[10] L. Liu, G. Moir, M. Peardon, S. M. Ryan, C. E. Thomas, P. Vilaseca, J. J. Dudek, R. G. Edwards, B. Joo, and

D. G. Richards (Hadron Spectrum Collaboration), J. High Energy Phys. 07 (2012) 126.
[11] Y. Chen, W.-F. Chiu, M. Gong, L.-C. Gui, and Z. Liu, Chin. Phys. C **40**, 081002 (2016).
[12] S. Ono, Z. Phys. C **26**, 307 (1984).
[13] E. Kou and O. Pene, Phys. Lett. B **631**, 164 (2005).
[14] Q.-F. Cao, H.-R. Qi, G.-Y. Tang, Y.-F. Xue, and H.-Q. Zheng, Eur. Phys. J. C **81**, 83 (2021).
[15] B.-Q. Li and K.-T. Chao, Phys. Rev. D **79**, 094004 (2009).
[16] F. J. Llanes-Estrada, Phys. Rev. D **72**, 031503 (2005).
[17] W. Qin, S.-R. Xue, and Q. Zhao, Phys. Rev. D **94**, 054035 (2016).
[18] F. Close and C. Downum, Phys. Rev. Lett. **102**, 242003 (2009).
[19] S. Coito and F. Giacosa, Acta Phys. Pol. B **51**, 1713 (2020).
[20] M. Ablikim *et al.* (BESIII Collaboration), Phys. Rev. Lett. **118**, 092001 (2017).
[21] M. Ablikim *et al.* (BESIII Collaboration), Phys. Rev. Lett. **118**, 092002 (2017).
[22] M. Ablikim *et al.* (BESIII Collaboration), Chin. Phys. C **46**, 111002 (2022).
[23] M. Ablikim *et al.* (BESIII Collaboration), Phys. Rev. D **107**, 092005 (2023).
[24] M. Ablikim *et al.* (BESIII Collaboration), Phys. Rev. D **96**, 032004 (2017); **99**, 019903(E) (2019).
[25] M. Ablikim *et al.* (BESIII Collaboration), Phys. Rev. D **109**, 092012 (2024).
[26] M. Ablikim *et al.* (BESIII Collaboration), Phys. Rev. D **99**, 091103 (2019).
[27] M. Ablikim *et al.* (BESIII Collaboration), Phys. Rev. Lett. **122**, 102002 (2019).
[28] M. Ablikim *et al.* (BESIII Collaboration), Phys. Rev. Lett. **131**, 151903 (2023).
[29] R. Oncala and J. Soto, Phys. Rev. D **96**, 014004 (2017).
[30] M. Ablikim *et al.* (BESIII Collaboration), Phys. Rev. D **96**, 012001 (2017).
[31] M. Ablikim *et al.* (BESIII Collaboration), Chin. Phys. C **39**, 093001 (2015).
[32] M. Ablikim *et al.* (BESIII Collaboration), Chin. Phys. C **40**, 063001 (2016).
[33] M. Ablikim *et al.* (BESIII Collaboration), Nucl. Instrum. Methods Phys. Res., Sect. A **614**, 345 (2010).
[34] S. Agostinelli *et al.* (GEANT4 Collaboration), Nucl. Instrum. Methods Phys. Res., Sect. A **506**, 250 (2003).
[35] J. Allison *et al.*, IEEE Trans. Nucl. Sci. **53**, 270 (2006).
[36] S. Jadach, B. F. L. Ward, and Z. Was, Comput. Phys. Commun. **130**, 260 (2000).
[37] R.-G. Ping, Chin. Phys. C **32**, 599 (2008).
[38] K. J. Peters, Int. J. Mod. Phys. A **21**, 5618 (2006).
[39] See Supplemental Material at http://link.aps.org/supplemental/10.1103/PhysRevD.111.L011101 for measurement of the $e^+e^- \to \eta h_c$ cross section from $\sqrt{s} =$ 4.130 to 4.600 GeV.
[40] H. Albrecht *et al.* (ARGUS Collaboration), Phys. Lett. B **241**, 278 (1990).
[41] S. Eidelman and F. Jegerlehner, Z. Phys. C **67**, 585 (1995).
[42] P. A. Zyla *et al.* (Particle Data Group), Prog. Theor. Exp. Phys. **2020**, 083C01 (2020).
[43] M. Ablikim *et al.* (BESIII Collaboration), Phys. Rev. Lett. **104**, 132002 (2010).
[44] S. Actis *et al.* (Working Group on Radiative Corrections, Monte Carlo Generators for Low Energies Collaboration), Eur. Phys. J. C **66**, 585 (2010).
[45] K. Stenson, arXiv:physics/0605236.
[46] R. L. Workman *et al.* (Particle Data Group), Prog. Theor. Exp. Phys. **2022**, 083C01 (2022).
[47] M. Berwein, N. Brambilla, J. Tarrús Castellà, and A. Vairo, Phys. Rev. D **92**, 114019 (2015).

M. Ablikim,[1] M. N. Achasov,[4,c] P. Adlarson,[75] O. Afedulidis,[3] X. C. Ai,[80] R. Aliberti,[35] A. Amoroso,[74a,74c] Q. An,[71,58,a] Y. Bai,[57] O. Bakina,[36] I. Balossino,[29a] Y. Ban,[46,h] H.-R. Bao,[63] V. Batozskaya,[1,44] K. Begzsuren,[32] N. Berger,[35] M. Berlowski,[44] M. Bertani,[28a] D. Bettoni,[29a] F. Bianchi,[74a,74c] E. Bianco,[74a,74c] A. Bortone,[74a,74c] I. Boyko,[36] R. A. Briere,[5] A. Brueggemann,[68] H. Cai,[76] X. Cai,[1,58] A. Calcaterra,[28a] G. F. Cao,[1,63] N. Cao,[1,63] S. A. Cetin,[62a] J. F. Chang,[1,58] G. R. Che,[43] G. Chelkov,[36,b] C. Chen,[43] C. H. Chen,[9] Chao Chen,[55] G. Chen,[1] H. S. Chen,[1,63] H. Y. Chen,[20] M. L. Chen,[1,58,63] S. J. Chen,[42] S. L. Chen,[45] S. M. Chen,[61] T. Chen,[1,63] X. R. Chen,[31,63] X. T. Chen,[1,63] Y. B. Chen,[1,58] Y. Q. Chen,[34] Z. J. Chen,[25,i] Z. Y. Chen,[1,63] S. K. Choi,[10] G. Cibinetto,[29a] F. Cossio,[74c] J. J. Cui,[50] H. L. Dai,[1,58] J. P. Dai,[78] A. Dbeyssi,[18] R. E. de Boer,[3] D. Dedovich,[36] C. Q. Deng,[72] Z. Y. Deng,[1] A. Denig,[35] I. Denysenko,[36] M. Destefanis,[74a,74c] F. De Mori,[74a,74c] B. Ding,[66,1] X. X. Ding,[46,h] Y. Ding,[34] Y. Ding,[40] J. Dong,[1,58] L. Y. Dong,[1,63] M. Y. Dong,[1,58,63] X. Dong,[76] M. C. Du,[1] S. X. Du,[80] Z. H. Duan,[42] P. Egorov,[36,b] Y. H. Fan,[45] J. Fang,[1,58] J. Fang,[59] S. S. Fang,[1,63] W. X. Fang,[1] Y. Fang,[1] Y. Q. Fang,[1,58] R. Farinelli,[29a] L. Fava,[74b,74c] F. Feldbauer,[3] G. Felici,[28a] C. Q. Feng,[71,58] J. H. Feng,[59] Y. T. Feng,[71,58] M. Fritsch,[3] C. D. Fu,[1] J. L. Fu,[63] Y. W. Fu,[1,63] H. Gao,[63] X. B. Gao,[41] Y. N. Gao,[46,h] Yang Gao,[71,58] S. Garbolino,[74c] I. Garzia,[29a,29b] L. Ge,[80] P. T. Ge,[76] Z. W. Ge,[42] C. Geng,[59] E. M. Gersabeck,[67] A. Gilman,[69] K. Goetzen,[13] L. Gong,[40] W. X. Gong,[1,58] W. Gradl,[35] S. Gramigna,[29a,29b] M. Greco,[74a,74c] M. H. Gu,[1,58] Y. T. Gu,[15] C. Y. Guan,[1,63] Z. L. Guan,[22] A. Q. Guo,[31,63] L. B. Guo,[41] M. J. Guo,[50] R. P. Guo,[49] Y. P. Guo,[12,g] A. Guskov,[36,b] J. Gutierrez,[27] K. L. Han,[63] T. T. Han,[1] X. Q. Hao,[19] F. A. Harris,[65] K. K. He,[55] K. L. He,[1,63] F. H. Heinsius,[3] C. H. Heinz,[35] Y. K. Heng,[1,58,63] C. Herold,[60] T. Holtmann,[3] P. C. Hong,[34] G. Y. Hou,[1,63] X. T. Hou,[1,63] Y. R. Hou,[63] Z. L. Hou,[1] B. Y. Hu,[59] H. M. Hu,[1,63] J. F. Hu,[56,j] S. L. Hu,[12,g] T. Hu,[1,58,63] Y. Hu,[1] G. S. Huang,[71,58] K. X. Huang,[59] L. Q. Huang,[31,63] X. T. Huang,[50] Y. P. Huang,[1]

T. Hussain,[73] F. Hölzken,[3] N. Hüsken,[27,35] N. in der Wiesche,[68] J. Jackson,[27] S. Janchiv,[32] J. H. Jeong,[10] Q. Ji,[1] Q. P. Ji,[19] W. Ji,[1,63] X. B. Ji,[1,63] X. L. Ji,[1,58] Y. Y. Ji,[50] X. Q. Jia,[50] Z. K. Jia,[71,58] D. Jiang,[1,63] H. B. Jiang,[76] P. C. Jiang,[46,h] S. S. Jiang,[39] T. J. Jiang,[16] X. S. Jiang,[1,58,63] Y. Jiang,[63] J. B. Jiao,[50] J. K. Jiao,[34] Z. Jiao,[23] S. Jin,[42] Y. Jin,[66] M. Q. Jing,[1,63] X. M. Jing,[63] T. Johansson,[75] S. Kabana,[33] N. Kalantar-Nayestanaki,[64] X. L. Kang,[9] X. S. Kang,[40] M. Kavatsyuk,[64] B. C. Ke,[80] V. Khachatryan,[27] A. Khoukaz,[68] R. Kiuchi,[1] O. B. Kolcu,[62a] B. Kopf,[3] M. Kuessner,[3] X. Kui,[1,63] N. Kumar,[26] A. Kupsc,[44,75] W. Kühn,[37] J. J. Lane,[67] P. Larin,[18] L. Lavezzi,[74a,74c] T. T. Lei,[71,58] Z. H. Lei,[71,58] M. Lellmann,[35] T. Lenz,[35] C. Li,[47] C. Li,[43] C. H. Li,[39] Cheng Li,[71,58] D. M. Li,[80] F. Li,[1,58] G. Li,[1] H. B. Li,[1,63] H. J. Li,[19] H. N. Li,[56,j] Hui Li,[43] J. R. Li,[61] J. S. Li,[59] Ke Li,[1] L. J. Li,[1,63] L. K. Li,[1] Lei Li,[48] M. H. Li,[43] P. R. Li,[38,l] Q. M. Li,[1,63] Q. X. Li,[50] R. Li,[17,31] S. X. Li,[12] T. Li,[50] W. D. Li,[1,63] W. G. Li,[1,a] X. Li,[1,63] X. H. Li,[71,58] X. L. Li,[50] X. Z. Li,[59] Xiaoyu Li,[1,63] Y. G. Li,[46,h] Z. J. Li,[59] Z. X. Li,[15] C. Liang,[42] H. Liang,[71,58] H. Liang,[1,63] Y. F. Liang,[54] Y. T. Liang,[31,63] G. R. Liao,[14] L. Z. Liao,[50] J. Libby,[26] A. Limphirat,[60] C. C. Lin,[55] D. X. Lin,[31,63] T. Lin,[1] B. J. Liu,[1] B. X. Liu,[76] C. Liu,[34] C. X. Liu,[1] F. H. Liu,[53] Fang Liu,[1] Feng Liu,[6] G. M. Liu,[56,j] H. Liu,[38,k,l] H. B. Liu,[15] H. M. Liu,[1,63] Huanhuan Liu,[1] Huihui Liu,[21] J. B. Liu,[71,58] J. Y. Liu,[1,63] K. Liu,[38,k,l] K. Y. Liu,[40] Ke Liu,[22] L. Liu,[71,58] L. C. Liu,[43] Lu Liu,[43] M. H. Liu,[12,g] P. L. Liu,[1] Q. Liu,[63] S. B. Liu,[71,58] T. Liu,[12,g] W. K. Liu,[43] W. M. Liu,[71,58] X. Liu,[39] X. Liu,[38,k,l] Y. Liu,[80] Y. Liu,[38,k,l] Y. B. Liu,[43] Z. A. Liu,[1,58,63] Z. D. Liu,[9] Z. Q. Liu,[50] X. C. Lou,[1,58,63] F. X. Lu,[59] H. J. Lu,[23] J. G. Lu,[1,58] X. L. Lu,[1] Y. Lu,[7] Y. P. Lu,[1,58] Z. H. Lu,[1,63] C. L. Luo,[41] M. X. Luo,[79] T. Luo,[12,g] X. L. Luo,[1,58] X. R. Lyu,[63] Y. F. Lyu,[43] F. C. Ma,[40] H. Ma,[78] H. L. Ma,[1] J. L. Ma,[1,63] L. L. Ma,[50] M. M. Ma,[1,63] Q. M. Ma,[1] R. Q. Ma,[1,63] T. Ma,[71,58] X. T. Ma,[1,63] X. Y. Ma,[1,58] Y. Ma,[46,h] Y. M. Ma,[31] F. E. Maas,[18] M. Maggiora,[74a,74c] S. Malde,[69] Y. J. Mao,[46,h] Z. P. Mao,[1] S. Marcello,[74a,74c] Z. X. Meng,[66] J. G. Messchendorp,[13,64] G. Mezzadri,[29a] H. Miao,[1,63] T. J. Min,[42] R. E. Mitchell,[27] X. H. Mo,[1,58,63] B. Moses,[27] N. Yu. Muchnoi,[4,c] J. Muskalla,[35] Y. Nefedov,[36] F. Nerling,[18,e] L. S. Nie,[20] I. B. Nikolaev,[4,c] Z. Ning,[1,58] S. Nisar,[11,m] Q. L. Niu,[38,k,l] W. D. Niu,[55] Y. Niu,[50] S. L. Olsen,[63] Q. Ouyang,[1,58,63] S. Pacetti,[28b,28c] X. Pan,[55] Y. Pan,[57] A. Pathak,[34] P. Patteri,[28a] Y. P. Pei,[71,58] M. Pelizaeus,[3] H. P. Peng,[71,58] Y. Y. Peng,[38,k,l] K. Peters,[13,e] J. L. Ping,[41] R. G. Ping,[1,63] S. Plura,[35] V. Prasad,[33] F. Z. Qi,[1] H. Qi,[71,58] H. R. Qi,[61] M. Qi,[42] T. Y. Qi,[12,g] S. Qian,[1,58] W. B. Qian,[63] C. F. Qiao,[63] X. K. Qiao,[80] J. J. Qin,[72] L. Q. Qin,[14] L. Y. Qin,[71,58] X. S. Qin,[50] Z. H. Qin,[1,58] J. F. Qiu,[1] Z. H. Qu,[72] C. F. Redmer,[35] K. J. Ren,[39] A. Rivetti,[74c] M. Rolo,[74c] G. Rong,[1,63] Ch. Rosner,[18] S. N. Ruan,[43] N. Salone,[44] A. Sarantsev,[36,d] Y. Schelhaas,[35] K. Schoenning,[75] M. Scodeggio,[29a] K. Y. Shan,[12,g] W. Shan,[24] X. Y. Shan,[71,58] Z. J. Shang,[38,k,l] J. F. Shangguan,[55] L. G. Shao,[1,63] M. Shao,[71,58] C. P. Shen,[12,g] H. F. Shen,[1,8] W. H. Shen,[63] X. Y. Shen,[1,63] B. A. Shi,[63] H. Shi,[71,58] H. C. Shi,[71,58] J. L. Shi,[12,g] J. Y. Shi,[1] Q. Q. Shi,[55] S. Y. Shi,[72] X. Shi,[1,58] J. J. Song,[19] T. Z. Song,[59] W. M. Song,[34,1] Y. J. Song,[12,g] Y. X. Song,[46,h,n] S. Sosio,[74a,74c] S. Spataro,[74a,74c] F. Stieler,[35] Y. J. Su,[63] G. B. Sun,[76] G. X. Sun,[1] H. Sun,[63] H. K. Sun,[1] J. F. Sun,[19] K. Sun,[61] L. Sun,[76] S. S. Sun,[1,63] T. Sun,[51,f] W. Y. Sun,[34] Y. Sun,[9] Y. J. Sun,[71,58] Y. Z. Sun,[1] Z. Q. Sun,[1,63] Z. T. Sun,[50] C. J. Tang,[54] G. Y. Tang,[1] J. Tang,[59] M. Tang,[71,58] Y. A. Tang,[76] L. Y. Tao,[72] Q. T. Tao,[25,i] M. Tat,[69] J. X. Teng,[71,58] V. Thoren,[75] W. H. Tian,[59] Y. Tian,[31,63] Z. F. Tian,[76] I. Uman,[62b] Y. Wan,[55] S. J. Wang,[50] B. Wang,[1] B. L. Wang,[63] Bo Wang,[71,58] D. Y. Wang,[46,h] F. Wang,[72] H. J. Wang,[38,k,l] J. J. Wang,[76] J. P. Wang,[50] K. Wang,[1,58] L. L. Wang,[1] M. Wang,[50] Meng Wang,[1,63] N. Y. Wang,[63] S. Wang,[38,k,l] S. Wang,[12,g] T. Wang,[12,g] T. J. Wang,[43] W. Wang,[59] W. Wang,[72] W. P. Wang,[35,71,o] X. Wang,[46,h] X. F. Wang,[38,k,l] X. J. Wang,[39] X. L. Wang,[12,g] X. N. Wang,[1] Y. Wang,[61] Y. D. Wang,[45] Y. F. Wang,[1,58,63] Y. L. Wang,[19] Y. N. Wang,[45] Y. Q. Wang,[1] Yaqian Wang,[17] Yi Wang,[61] Z. Wang,[1,58] Z. L. Wang,[72] Z. Y. Wang,[1,63] Ziyi Wang,[63] D. H. Wei,[14] F. Weidner,[68] S. P. Wen,[1] Y. R. Wen,[39] U. Wiedner,[3] G. Wilkinson,[69] M. Wolke,[75] L. Wollenberg,[3] C. Wu,[39] J. F. Wu,[1,8] L. H. Wu,[1] L. J. Wu,[1,63] X. Wu,[12,g] X. H. Wu,[34] Y. Wu,[71,58] Y. H. Wu,[55] Y. J. Wu,[31] Z. Wu,[1,58] L. Xia,[71,58] X. M. Xian,[39] B. H. Xiang,[1,63] T. Xiang,[46,h] D. Xiao,[38,k,l] G. Y. Xiao,[42] S. Y. Xiao,[1] Y. L. Xiao,[12,g] Z. J. Xiao,[41] C. Xie,[42] X. H. Xie,[46,h] Y. Xie,[50] Y. G. Xie,[1,58] Y. H. Xie,[6] Z. P. Xie,[71,58] T. Y. Xing,[1,63] C. F. Xu,[1,63] C. J. Xu,[59] G. F. Xu,[1] H. Y. Xu,[66] M. Xu,[71,58] Q. J. Xu,[16] Q. N. Xu,[30] W. Xu,[1] W. L. Xu,[66] X. P. Xu,[55] Y. C. Xu,[77] Z. P. Xu,[42] Z. S. Xu,[63] F. Yan,[12,g] L. Yan,[12,g] W. B. Yan,[71,58] W. C. Yan,[80] X. Q. Yan,[1] H. J. Yang,[51,f] H. L. Yang,[34] H. X. Yang,[1] Tao Yang,[1] Y. Yang,[12,g] Y. F. Yang,[43] Y. X. Yang,[1,63] Yifan Yang,[1,63] Z. W. Yang,[38,k,l] Z. P. Yao,[50] M. Ye,[1,58] M. H. Ye,[8] J. H. Yin,[1] Z. Y. You,[59] B. X. Yu,[1,58,63] C. X. Yu,[43] G. Yu,[1,63] J. S. Yu,[25,i] T. Yu,[72] X. D. Yu,[46,h] Y. C. Yu,[80] C. Z. Yuan,[1,63] J. Yuan,[34] L. Yuan,[2] S. C. Yuan,[1] Y. Yuan,[1,63] Y. J. Yuan,[45] Z. Y. Yuan,[59] C. X. Yue,[39] A. A. Zafar,[73] F. R. Zeng,[50] S. H. Zeng,[72] X. Zeng,[12,g] Y. Zeng,[25,i] Y. J. Zeng,[59] X. Y. Zhai,[34] Y. C. Zhai,[50] Y. H. Zhan,[59] A. Q. Zhang,[1,63] B. L. Zhang,[1,63] B. X. Zhang,[1] D. H. Zhang,[43] G. Y. Zhang,[19] H. Zhang,[71,58] H. Zhang,[80] H. C. Zhang,[1,58,63] H. H. Zhang,[59] H. H. Zhang,[34] H. Q. Zhang,[1,58,63] H. R. Zhang,[71,58] H. Y. Zhang,[1,58] J. Zhang,[59] J. Zhang,[80] J. J. Zhang,[52] J. L. Zhang,[20] J. Q. Zhang,[41] J. S. Zhang,[12,g] J. W. Zhang,[1,58,63] J. X. Zhang,[38,k,l] J. Y. Zhang,[1] J. Z. Zhang,[1,63] Jianyu Zhang,[63] L. M. Zhang,[61] Lei Zhang,[42] P. Zhang,[1,63] Q. Y. Zhang,[34] R. Y. Zhang,[38,k,l] Shuihan Zhang,[1,63] Shulei Zhang,[25,i] X. D. Zhang,[45] X. M. Zhang,[1] X. Y. Zhang,[50] Y. Zhang,[72] Y. T. Zhang,[80] Y. H. Zhang,[1,58] Y. M. Zhang,[39] Yan Zhang,[71,58] Yao Zhang,[1] Z. D. Zhang,[1] Z. H. Zhang,[1] Z. L. Zhang,[34] Z. Y. Zhang,[43] Z. Y. Zhang,[76] Z. Z. Zhang,[45] G. Zhao,[1] J. Y. Zhao,[1,63] J. Z. Zhao,[1,58] Lei Zhao,[71,58] Ling Zhao,[1] M. G. Zhao,[43] N. Zhao,[78] R. P. Zhao,[63] S. J. Zhao,[80] Y. B. Zhao,[1,58] Y. X. Zhao,[31,63] Z. G. Zhao,[71,58] A. Zhemchugov,[36,b] B. Zheng,[72] B. M. Zheng,[34] J. P. Zheng,[1,58] W. J. Zheng,[1,63] Y. H. Zheng,[63] B. Zhong,[41] X. Zhong,[59] H. Zhou,[50] J. Y. Zhou,[34] L. P. Zhou,[1,63] S. Zhou,[6] X. Zhou,[76] X. K. Zhou,[6] X. R. Zhou,[71,58] X. Y. Zhou,[39] Y. Z. Zhou,[12,g] J. Zhu,[43] K. Zhu,[1] K. J. Zhu,[1,58,63] K. S. Zhu,[12,g] L. Zhu,[34] L. X. Zhu,[63] S. H. Zhu,[70] S. Q. Zhu,[42] T. J. Zhu,[12,g] W. D. Zhu,[41] Y. C. Zhu,[71,58] Z. A. Zhu,[1,63] J. H. Zou,[1] and J. Zu[71,58]

(BESIII Collaboration)

[1]*Institute of High Energy Physics, Beijing 100049, People's Republic of China*
[2]*Beihang University, Beijing 100191, People's Republic of China*
[3]*Bochum Ruhr-University, D-44780 Bochum, Germany*
[4]*Budker Institute of Nuclear Physics SB RAS (BINP), Novosibirsk 630090, Russia*
[5]*Carnegie Mellon University, Pittsburgh, Pennsylvania 15213, USA*
[6]*Central China Normal University, Wuhan 430079, People's Republic of China*
[7]*Central South University, Changsha 410083, People's Republic of China*
[8]*China Center of Advanced Science and Technology, Beijing 100190, People's Republic of China*
[9]*China University of Geosciences, Wuhan 430074, People's Republic of China*
[10]*Chung-Ang University, Seoul, 06974, Republic of Korea*
[11]*COMSATS University Islamabad, Lahore Campus, Defence Road, Off Raiwind Road, 54000 Lahore, Pakistan*
[12]*Fudan University, Shanghai 200433, People's Republic of China*
[13]*GSI Helmholtzcentre for Heavy Ion Research GmbH, D-64291 Darmstadt, Germany*
[14]*Guangxi Normal University, Guilin 541004, People's Republic of China*
[15]*Guangxi University, Nanning 530004, People's Republic of China*
[16]*Hangzhou Normal University, Hangzhou 310036, People's Republic of China*
[17]*Hebei University, Baoding 071002, People's Republic of China*
[18]*Helmholtz Institute Mainz, Staudinger Weg 18, D-55099 Mainz, Germany*
[19]*Henan Normal University, Xinxiang 453007, People's Republic of China*
[20]*Henan University, Kaifeng 475004, People's Republic of China*
[21]*Henan University of Science and Technology, Luoyang 471003, People's Republic of China*
[22]*Henan University of Technology, Zhengzhou 450001, People's Republic of China*
[23]*Huangshan College, Huangshan 245000, People's Republic of China*
[24]*Hunan Normal University, Changsha 410081, People's Republic of China*
[25]*Hunan University, Changsha 410082, People's Republic of China*
[26]*Indian Institute of Technology Madras, Chennai 600036, India*
[27]*Indiana University, Bloomington, Indiana 47405, USA*
[28a]*INFN Laboratori Nazionali di Frascati, I-00044, Frascati, Italy*
[28b]*INFN Sezione di Perugia, I-06100, Perugia, Italy*
[28c]*University of Perugia, I-06100, Perugia, Italy*
[29a]*INFN Sezione di Ferrara, INFN Sezione di Ferrara, I-44122, Ferrara, Italy*
[29b]*University of Ferrara, I-44122, Ferrara, Italy*
[30]*Inner Mongolia University, Hohhot 010021, People's Republic of China*
[31]*Institute of Modern Physics, Lanzhou 730000, People's Republic of China*
[32]*Institute of Physics and Technology, Peace Avenue 54B, Ulaanbaatar 13330, Mongolia*
[33]*Instituto de Alta Investigación, Universidad de Tarapacá, Casilla 7D, Arica 1000000, Chile*
[34]*Jilin University, Changchun 130012, People's Republic of China*
[35]*Johannes Gutenberg University of Mainz, Johann-Joachim-Becher-Weg 45, D-55099 Mainz, Germany*
[36]*Joint Institute for Nuclear Research, 141980 Dubna, Moscow region, Russia*
[37]*Justus-Liebig-Universitaet Giessen, II. Physikalisches Institut, Heinrich-Buff-Ring 16, D-35392 Giessen, Germany*
[38]*Lanzhou University, Lanzhou 730000, People's Republic of China*
[39]*Liaoning Normal University, Dalian 116029, People's Republic of China*
[40]*Liaoning University, Shenyang 110036, People's Republic of China*
[41]*Nanjing Normal University, Nanjing 210023, People's Republic of China*
[42]*Nanjing University, Nanjing 210093, People's Republic of China*
[43]*Nankai University, Tianjin 300071, People's Republic of China*

[44]*National Centre for Nuclear Research, Warsaw 02-093, Poland*
[45]*North China Electric Power University, Beijing 102206, People's Republic of China*
[46]*Peking University, Beijing 100871, People's Republic of China*
[47]*Qufu Normal University, Qufu 273165, People's Republic of China*
[48]*Renmin University of China, Beijing 100872, People's Republic of China*
[49]*Shandong Normal University, Jinan 250014, People's Republic of China*
[50]*Shandong University, Jinan 250100, People's Republic of China*
[51]*Shanghai Jiao Tong University, Shanghai 200240, People's Republic of China*
[52]*Shanxi Normal University, Linfen 041004, People's Republic of China*
[53]*Shanxi University, Taiyuan 030006, People's Republic of China*
[54]*Sichuan University, Chengdu 610064, People's Republic of China*
[55]*Soochow University, Suzhou 215006, People's Republic of China*
[56]*South China Normal University, Guangzhou 510006, People's Republic of China*
[57]*Southeast University, Nanjing 211100, People's Republic of China*
[58]*State Key Laboratory of Particle Detection and Electronics, Beijing 100049, Hefei 230026, People's Republic of China*
[59]*Sun Yat-Sen University, Guangzhou 510275, People's Republic of China*
[60]*Suranaree University of Technology, University Avenue 111, Nakhon Ratchasima 30000, Thailand*
[61]*Tsinghua University, Beijing 100084, People's Republic of China*
[62a]*Turkish Accelerator Center Particle Factory Group, Istinye University, 34010, Istanbul, Turkey*
[62b]*Near East University, Nicosia, North Cyprus, 99138, Mersin 10, Turkey*
[63]*University of Chinese Academy of Sciences, Beijing 100049, People's Republic of China*
[64]*University of Groningen, NL-9747 AA Groningen, The Netherlands*
[65]*University of Hawaii, Honolulu, Hawaii 96822, USA*
[66]*University of Jinan, Jinan 250022, People's Republic of China*
[67]*University of Manchester, Oxford Road, Manchester, M13 9PL, United Kingdom*
[68]*University of Muenster, Wilhelm-Klemm-Strasse 9, 48149 Muenster, Germany*
[69]*University of Oxford, Keble Road, Oxford OX13RH, United Kingdom*
[70]*University of Science and Technology Liaoning, Anshan 114051, People's Republic of China*
[71]*University of Science and Technology of China, Hefei 230026, People's Republic of China*
[72]*University of South China, Hengyang 421001, People's Republic of China*
[73]*University of the Punjab, Lahore-54590, Pakistan*
[74a]*University of Turin and INFN, University of Turin, I-10125, Turin, Italy*
[74b]*University of Eastern Piedmont, I-15121, Alessandria, Italy*
[74c]*INFN, I-10125, Turin, Italy*
[75]*Uppsala University, Box 516, SE-75120 Uppsala, Sweden*
[76]*Wuhan University, Wuhan 430072, People's Republic of China*
[77]*Yantai University, Yantai 264005, People's Republic of China*
[78]*Yunnan University, Kunming 650500, People's Republic of China*
[79]*Zhejiang University, Hangzhou 310027, People's Republic of China*
[80]*Zhengzhou University, Zhengzhou 450001, People's Republic of China*

[a]Deceased.
[b]Also at the Moscow Institute of Physics and Technology, Moscow 141700, Russia.
[c]Also at the Novosibirsk State University, Novosibirsk, 630090, Russia.
[d]Also at the NRC "Kurchatov Institute," PNPI, 188300, Gatchina, Russia.
[e]Also at Goethe University Frankfurt, 60323 Frankfurt am Main, Germany.
[f]Also at Key Laboratory for Particle Physics, Astrophysics and Cosmology, Ministry of Education; Shanghai Key Laboratory for Particle Physics and Cosmology; Institute of Nuclear and Particle Physics, Shanghai 200240, People's Republic of China.
[g]Also at Key Laboratory of Nuclear Physics and Ion-beam Application (MOE) and Institute of Modern Physics, Fudan University, Shanghai 200443, People's Republic of China.
[h]Also at State Key Laboratory of Nuclear Physics and Technology, Peking University, Beijing 100871, People's Republic of China.
[i]Also at School of Physics and Electronics, Hunan University, Changsha 410082, China.
[j]Also at Guangdong Provincial Key Laboratory of Nuclear Science, Institute of Quantum Matter, South China Normal University, Guangzhou 510006, China.
[k]Also at MOE Frontiers Science Center for Rare Isotopes, Lanzhou University, Lanzhou 730000, People's Republic of China.
[l]Also at Lanzhou Center for Theoretical Physics, Lanzhou University, Lanzhou 730000, People's Republic of China.
[m]Also at the Department of Mathematical Sciences, IBA, Karachi 75270, Pakistan.
[n]Also at Ecole Polytechnique Federale de Lausanne (EPFL), CH-1015 Lausanne, Switzerland.
[o]Also at Helmholtz Institute Mainz, Staudinger Weg 18, D-55099 Mainz, Germany.